Journal of Power Sources 216 (2012) 187–191

Contents lists available at SciVerse ScienceDirect

Journal of Power Sources

journal homepage: www.elsevier.com/locate/jpowsour

Short communication

MnO_2–graphene hybrid as an alternative cathodic catalyst to platinum in microbial fuel cells

Qing Wen, Shaoyun Wang, Jun Yan, Lijie Cong, Zhongcheng Pan, Yueming Ren, Zhuangjun Fan*

Key Laboratory of Super-light Materials & Surface Technology, Ministry of Education, College of Material Science and Chemical Engineering, Harbin Engineering University, Harbin 150001, China

HIGHLIGHTS

- MnO_2–graphene nanosheet (MnO_2/GNS) hybrid is prepared under microwave irradiation.
- The electrode modified by MnO_2/GNS exhibits high catalytic activity for ORR.
- Microbial fuel cells with MnO_2/GNS generates a maximum power density of 2083 mW m^{-2}.

ARTICLE INFO

Article history:
Received 5 May 2012
Accepted 10 May 2012
Available online 28 May 2012

Keywords:
Microbial fuel cell
Graphene
Manganese dioxide–graphene hybrid
Oxygen reduction reaction

ABSTRACT

Manganese dioxide–graphene nanosheet (MnO_2/GNS) hybrid is used as an alternative cathode catalyst for oxygen reduction reaction in air-cathode microbial fuel cell (MFC). The results show that the nanostructured MnO_2/GNS composite exhibit an excellent catalytic activity for oxygen reduction reaction due to MnO_2 nanoparticles closely anchored on the excellent conductive graphene nanosheets. As a result, MFC with MnO_2/GNS as air cathode catalyst generates a maximum power density of 2083 mW m^{-2}, which is higher than that of MFC with pure manganese dioxide catalyst (1470 mW m^{-2}). Therefore, MnO_2/GNS nanocomposite is an efficient and cost-effective cathode catalyst for practical MFC applications.

1. Introduction

Microbial fuel cells (MFCs) utilize microorganisms as catalysts to decompose organic or inorganic matter and then harvest electricity, which represents a novel and promising technology for the generation of alternative power and wastewater treatment [1]. Although the research on MFC has been increased rapidly, there are still many challenges, especially with respect to the cathode, whose performance should be further ameliorated. Oxygen has been considered as one of the most suitable electron acceptors in MFCs due to its limitless availability and high redox potential among many kinds of cathodic electron acceptors. However, the sluggish kinetics of the oxygen reduction reaction (ORR) in a near neutral medium seriously limits the power density production of MFCs [2,3]. In order to overcome this problem, platinum has been widely used to enhance the ORR in MFCs. Wang et al. coated Pt nanoparticles on the surface of carbon nanotubes (CNTs) to improve the activity of the catalyst. As a consequence, the performance of the MFC was improved significantly [4]. However, the practical application of platinum has been limited greatly due to its relatively high cost and sensitivity to poisoning [5,6].

Recently, various non-noble metal based catalysts have been investigated as cathodic catalysts for MFCs, such as iron phthalocyanine [7], Co-naphthalocyanine (CoNPc) [8], Co/Fe/N/CNT [9], manganese dioxide [10,11] and so on, aiming to lower the cost of cathodes and simultaneously improve ORR kinetics. Among these materials, manganese dioxide is considered as a successful cathode catalyst for ORR in MFCs owing to its low cost and toxicity, environmental benignity, and high chemical stability and catalytic activity [12,13].

The studies of MnO_2 applied in MFCs suggested that the crystal structure, particle size, synthesis method and the support material of MnO_2 catalyst could significantly affect the catalytic activity of MnO_2. For example, MnO_2 materials with different crystal structure (α-MnO_2, β-MnO_2, and γ-MnO_2) have been investigated extensively as the cathode catalysts in MFCs, β-MnO_2 was proved to be the most effective catalyst with a maximum power density of 466 $\pm$ 19 mW m^{-3} [14]. X. W. Liu et al. [15] employed a nanostructured MnO_2, which was prepared by an electrochemical deposition method, as an effective ORR cathodic catalyst in an MFC

* Corresponding author. Tel./fax: +86 451 82569890.
E-mail address: fanzhj666@163.com (Z. Fan).

0378-7753/$ – see front matter © 2012 Elsevier B.V. All rights reserved.
doi:10.1016/j.jpowsour.2012.05.023

to generate a maximum power density of 772.8 mW m^{-3}. However, due to poor dispersion and electrical conductivity of MnO_2, the electrochemical performance of pure MnO_2 is still unsatisfactory. As an effective solution, MnO_2 can be incorporated into the electron-conductive materials (such as carbon) to improve its catalytic activity for ORR. Previous approaches to the synthesis of MnO_2/carbon composite mainly included physical mixing, thermal decomposition, ball milling, electrodeposition, chemical deposition using precursors such as permanganate and so on. For example, a maximum power density of 210 mW m^{-2} produced from the MFC with MnO_2/CNTs cathode catalyst synthesized by a hydrothermal method was slightly lower than that of the MFC with a Pt/C cathode (229 mW m^{-2}) [16]. Interestingly, Fischer AE et al. [17] described the self-limiting deposition of nanoscale MnO_2 onto carbon nanofoam. In this method, the carbon substrate acted as a substrate as well as a reductant to convert aqueous permanganate (MnO_4^-) to insoluble MnO_2. All reports demonstrated that the electrochemical performance of such MnO_2/carbon structure was largely affected by the morphology and distribution of the MnO_2 phase. In addition, the structure of the carbon substrate was another important influencing factor.

Graphene nanosheet (GNS) is a kind of two-dimensional layer of sp^2 hybridized carbon, which has the outstanding physical and chemical properties, such as high electrical conductivity, thermal stability, and large surface area. The individual nanosheet does not depend on the distribution of pores in a solid to give its large surface area [18], so GNS has significant advantages for catalyst support material compared with the conventional carbon materials such as activated carbon and CNTs. Recently, Xiao et al. has demonstrated that the crumpled graphene particles can be employed as effective electrode modifying materials for improving electricity generation in MFCs. The obtained maximum power densities with the crumpled graphene and flat graphene modified cathode electrodes were 3.3 W m^{-3} and 2.5 W m^{-3}, respectively, significantly higher than 0.3 W m^{-3} with the unmodified carbon cloth [19].

To our knowledge, there are few works on the nanostructured MnO_2/GNS composite as a cathode catalyst for ORR in MFCs. In this paper, MnO_2 functionalized GNS (MnO_2/GNS) was prepared by a direct redox reaction between graphene and potassium permanganate under microwave irradiation. In this process, GNS acts as both a reducing agent and a highly conductive substrate for the self-limiting deposition of MnO_2 in an aqueous $KMnO_4$ solution. Moreover, the strong interaction and the increased contact area between MnO_2 and GNS could greatly promote the catalyst stability and the electrical conductivity due to the high electrical conductivity of GNS. Therefore, nanoscale MnO_2/GNS composite with excellent electrical conductivity, small particle size and high catalytic performance can be obtained through this method and would exhibit a high catalytic activity for ORR in MFCs.

In the present study, the synthesis of MnO_2/GNS nanocomposite was prepared as mentioned above. The catalyst characterization was investigated through transmission electron microscopy (TEM) and X-ray diffraction (XRD) and the evaluation on the ORR activity of the MnO_2/GNS nanocomposite was investigated through cyclic voltammograms (CV) and electrochemical impedance spectroscopy (EIS). Further performance examination was evaluated in an MFC with MnO_2/GNS catalyst air cathode.

2. Experimental

2.1. Catalyst preparation

Graphite oxide was synthesized from natural graphite by a modified Hummers method [20]. The GNS was synthesized by hydrazine reduction of graphite oxide as described elsewhere [21]. MnO_2/GNS composite was prepared by a redox reaction between GNS and potassium permanganate under microwave irradiation. Specifically, 0.165 mg of GNS was added into 100 mL distilled water and subjected by ultrasonic vibration for 1 h. Then 0.5972 g of $KMnO_4$ powder was added into the GNS suspension prepared before. After being stirred for 10 min, the mixture was heated using a household microwave oven (Haier, 2450 MHz, 700 W) for 5 min, and then cooled to room temperature naturally. Subsequently, the black precipitate (MnO_2/GNS) was separated by filter separator and washed several times with distilled water and alcohol, then dried for 12 h in a vacuum oven at 100 °C.

2.2. Electrode preparation

The air cathode was manufactured by pressing wet-proof gas diffusion layers (50 wt% Na_2SO_4 and 50 wt% polytetrafluoroethylene (PTFE)), catalyst layer (86 wt% activated carbon powder, 12 wt% PTFE, and 2 wt% acetylene black powder, containing 5 mg cm^{-2} MnO_2/GNS catalyst) and stainless steel net. As controls, the Pt/C, MnO_2 catalyst and none catalyst air cathodes were fabricated using the same procedure. MnO_2 catalyst was loaded onto the air cathode at 5 mg cm^{-2} and the Pt/C catalyst was loaded at 0.5 mg cm^{-2}. In order to investigate the ORR performance, CV and EIS were performed in a three-electrode configuration. The working electrodes were prepared as follows: 4.3 mg of acetylene black was added into 20 mL of alcohol and then subjected to ultrasonic vibration for 1 h. Subsequently, 10 mg of catalyst (MnO_2 or MnO_2/GNS) and 0.015 mL of PTFE (0.1 g mL^{-1}) was added into the resulting suspension, and then heated by electric furnace until it became a paste. Finally, each catalyst paste was pasted onto carbon paper (2 cm^2) by brush and then dried at a room temperature for 48 h.

2.3. MFC construction and operation

The air-cathode single chamber MFC was built with a cylindrical plastic tube, which had an inner diameter of 6 cm and total height of 8 cm. The air cathode (5 × 2 cm^2) was placed on one side of the outer surface of the MFC, whereas the anode was cylindrical carbon felt (78 cm^2). Two electrodes were separated by 1 cm. For comparing the performance of MFCs with different cathode catalysts, four air-cathode single chamber MFC reactors with MnO_2, MnO_2/GNS, Pt/C and none catalyst air cathodes, were set up for the experiments. For each type of catalyst, MFCs in duplicates were tested simultaneously. MFC reactors were inoculated using anaerobic sludge collected from another MFC which had been operated continuously in our lab. MFC reactors were operated using nutrient buffer solution (NBS) containing the following: acetate, 1 g L^{-1}; KCl, 130 mg L^{-1}; $NaH_2PO_4 \cdot 2H_2O$, 4.97 g L^{-1}; $Na_2HPO_4 \cdot 12H_2O$, 2.75 g L^{-1}; and other trace elements required for microorganism growth as reported by Liu and Logan [22]. The nutrient buffer solution (200 mL) was refreshed when the voltage decreased to below 50 mV, forming a fed-batch. All experiments were conducted at a room temperature (24 ± 1 °C).

2.4. Analysis and calculation

The output voltage was measured across an external resistor (1500 Ω resistor except where indicated otherwise) using a data acquisition system connected to a computer. Polarization curve of MFCs and the performance of the electrode potential were measured as previously described [23]. Current density and power density were normalized to the geometric surface of the cathode (10 cm^2).

To electrochemically characterize the catalyst, CV and EIS were performed using an electrochemical workstation (SP-240, Bio-Logic), with a three-electrode configuration consisting of an Ag/AgCl reference electrode, a working electrode (the catalyst-modified carbon papers), and a platinum foil counter electrode placed in 50 mmol L^{-1} phosphate buffered solution aerated by oxygen for 1.5 h. EIS was performed over a frequency range of 200,000 to 0.1 Hz at open-circuit condition with a perturbation signal of 5 mV.

3. Results and discussion

3.1. Microstructure of MnO_2/GNS

MnO_2/GNS composite was synthesized through a redox reaction between GNS and potassium permanganate under microwave irradiation. MnO_2 nanoparticles grown on GNS depended on the direct redox reaction as follows:

$$4MnO_4^- + 3C + H_2O \rightleftharpoons 4MnO_2 + CO_3^{2-} + 2HCO_3^- \quad (1)$$

As shown in Fig. 1, nanoscale MnO_2 particles with the size of about 5–10 nm and an interlayer spacing of 0.7 nm were coated uniformly on the surface of GNS. X-ray diffraction analysis confirmed the monoclinic lamellar structure of birnessite-type MnO_2 (JCPDS 42–1317) (Fig. 2) [24]. Moreover, BET surface area of MnO_2/GNS (158.29 m^2 g^{-1}) was higher than that of MnO_2 (40.64 m^2 g^{-1}), meaning the uniform dispersion of MnO_2 nanoparticles on the sheet.

3.2. Electrochemical performance

The oxygen reduction characteristics of the electrode with MnO_2/GNS catalyst alongside those of the electrodes with Pt/C catalyst, MnO_2 catalyst and non-catalyst were analyzed by CV and EIS to determine whether the MnO_2/GNS contributes to the catalytic reaction. Fig. 3A shows the results of the CV for the electrodes with different catalysts. At the potential of −0.43 V, the current of the ORR at the electrode with MnO_2/GNS catalyst is −14.23 mA, which is 4.20 times that of the electrode with MnO_2 catalyst (−3.39 mA) and 8.22 times that of the electrode with non-catalyst (−1.73 mA). Obvious oxygen reduction peak of the electrode with MnO_2/GNS catalyst is clearly observed at −0.43 V, which is more positive than that of MnO_2 catalyst (−0.71 V) and even a little more positive than that of Pt/C catalyst (−0.44 V), indicating that MnO_2/GNS could catalyze ORR at a more positive potential. Moreover, the oxygen reduction peak current of MnO_2/GNS catalyst is bigger than that of Pt/C catalyst. The increase of the current and peak potential for the electrode with MnO_2/GNS catalyst demonstrates the higher catalytic activity of MnO_2/GNS toward oxygen reduction than those of the controls. The active catalytic property of MnO_2/GNS can be attributed to the large catalyst surface area, which is provided by the nanoscale size of the MnO_2 catalyst particles (5–10 nm) and the high degree of homogeneous dispersion of MnO_2 on the surface of the GNS. Fig. 3B shows the CV of MnO_2/GNS electrode at different scan rates (10, 15, and 20 mV s^{-1}). The electrode peak current is linearly (R^2 = 0.9942) proportional to the square root of the scan rates, indicating that the redox reaction is a diffusion controlled process and confirming that the immobilized MnO_2/GNS is rather stable.

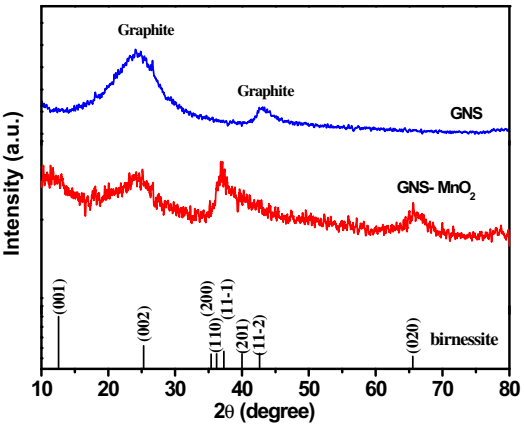

Fig. 2. XRD patterns of graphene and MnO_2/GNS composites.

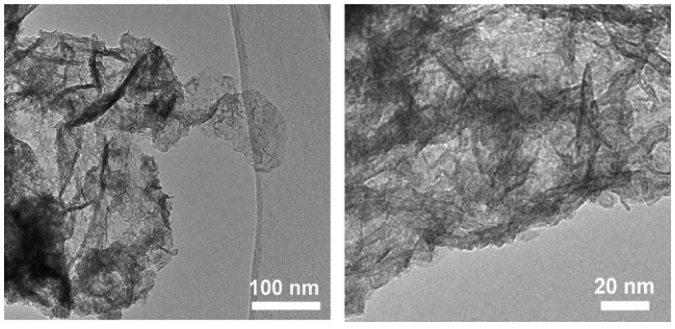

Fig. 1. TEM image of MnO_2/GNS composite.

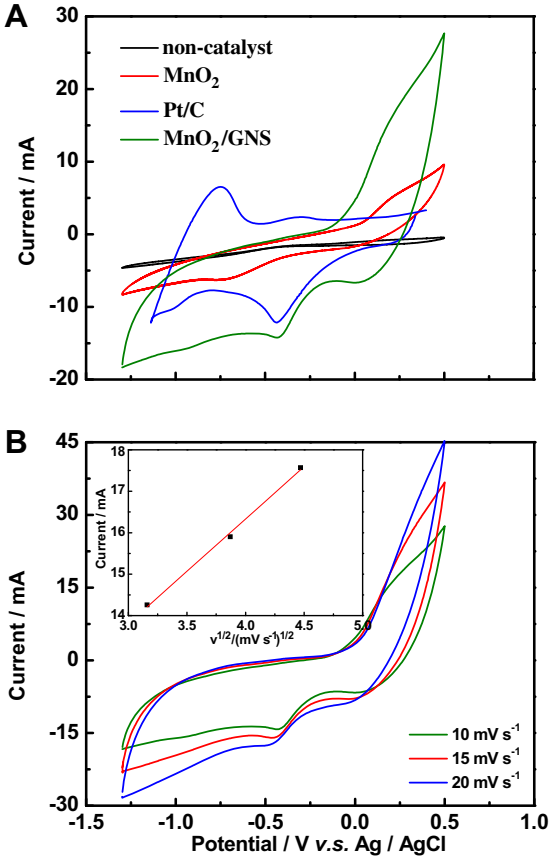

Fig. 3. Cyclic voltammograms of (A) The electrodes with different catalysts at scan rate of 10 mV s^{-1}, and (B) The electrode with MnO_2/GNS catalyst at the scan rate (from inner to outer) 10,15, and 20 mV s^{-1} in 50 mmol L^{-1} phosphate buffered solution (pH = 7.0).

The Nyquist plots were measured on the electrodes with different catalysts (Fig. 4). The insert in Fig. 4 shows the EIS of MnO_2, Pt/C and MnO_2/GNS electrodes. All the Nyquist plots of the electrodes with different catalysts represent a well-defined frequency-dependent semicircle impedance curve over high frequency followed by a straight line. The total resistance order of the electrodes with different catalysts is non-catalyst (133.7 Ω) > MnO_2 (29.02 Ω) > Pt/C (16.4 Ω) > MnO_2/GNS (12.4 Ω). The charge-transfer resistance (R_{ct}) is equal to the diameter of the semicircle. A faster electron-transfer rate could be indicated by a smaller R_{ct}. The value of R_{ct} for the electrode with MnO_2/GNS catalyst is the smallest, indicating that MnO_2/GNS catalyst greatly reduces the electron-transfer resistance and increases the reaction rate. The result could be explained by the great catalyst surface area and the high conductivity of MnO_2/GNS due to the high electrical conductivity of GNS. Moreover, the excellent interfacial contact and the increased contact area between MnO_2 and GNS could be of great benefit to fast transportation of electron throughout the whole electrode matrix. The diffusion-limiting step in an electrochemical process is usually evaluated by the straight line region [25]. The straight line region over low frequency of MnO_2/GNS electrode after the high frequency-dependent semicircle is significantly smaller than that of non-catalyst, MnO_2 and Pt/C electrodes. It has been indicated that the diffusion resistance for ORR is reduced greatly, likely due to the peculiar two-dimensional layers structure of GNS. Therefore, both CV and EIS results demonstrate that the MnO_2/GNS nanocomposite has high catalytic activity for ORR.

3.3. The performance of MFCs with different cathode catalysts

The cell voltage curves, anode and cathode polarization curves, and power density curves were evaluated in MFCs with MnO_2/GNS, MnO_2, Pt/C and non-catalyst air cathodes. The performance order of MFCs with different cathodes is MnO_2/GNS > Pt/C > MnO_2 > non-catalyst cathode as illustrated in Fig. 5. The maximum power density of the MFC with MnO_2/GNS catalyst air cathode at a loading of 5.0 mg cm^{-2} is 2084 mW m^{-2} (10.42 W m^{-3}) (Fig. 5A), which is higher than that of MnO_2 catalyst air cathode (1470 mW m^{-2}) and non-catalyst cathode (333 mW m^{-2}), and even higher than that of Pt/C cathode at a loading of 0.5 mg cm^{-2} (1714 mW m^{-2}). The result suggests that the MnO_2/GNS cathodes perform a high catalytic activity and improved the power generation. As shown in Fig. 5B, the open circuit voltage (OCV) of the MFC with MnO_2/GNS cathode at a loading of 5.0 mg cm^{-2} is 0.771 V, which is improved by 7.1%

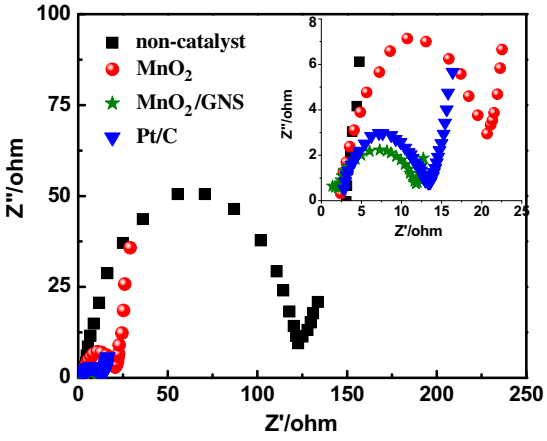

Fig. 4. EIS of different catalysts assembled on carbon paper electrode in 50 mmol L^{-1} phosphate buffered solution (pH = 7.0).

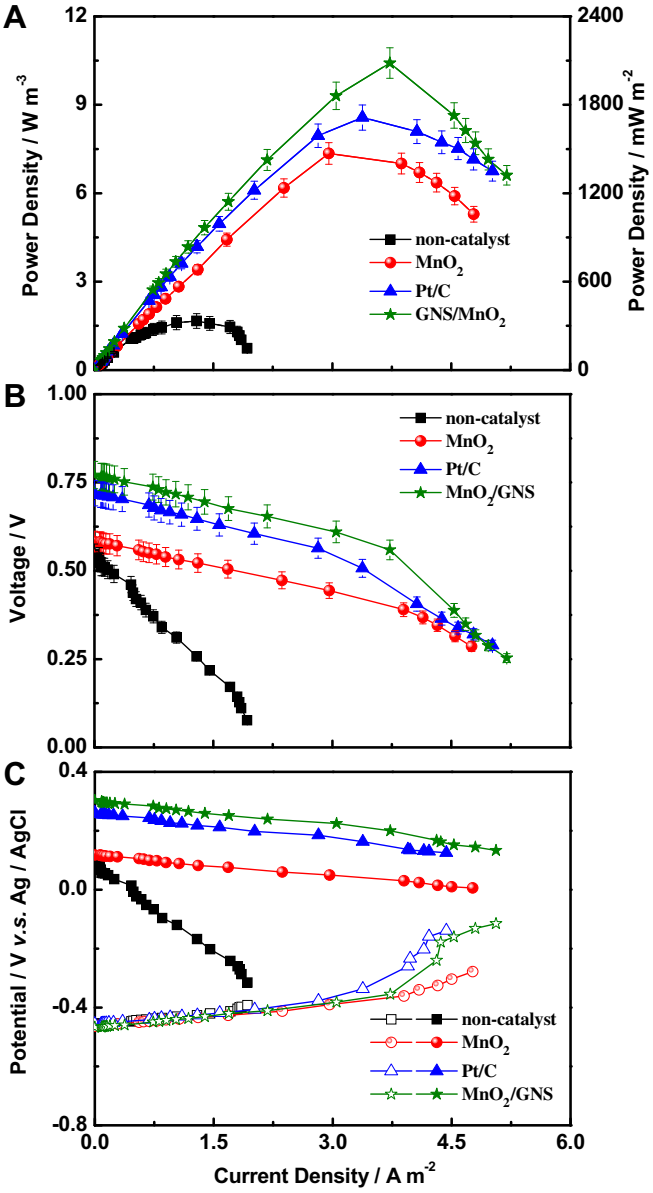

Fig. 5. Performance of MFC equipped with non-catalyst cathode, MnO_2 cathode, Pt/C cathode and MnO_2/GNS cathode: (A) power density curves, (B) cell voltage curves, and (C) anode and cathode polarization curves (cathode: filled symbols; anode: open symbols).

when compared with Pt/C cathode at a loading of 0.5 mg cm^{-2} (0.720 V), and much higher than that of MnO_2 cathode at a loading of 5.0 mg cm^{-2} (0.583 V) and non-catalyst cathode (0.548 V). Curves of the individual cathode or anode potential versus current density are shown in Fig. 5C. The anode potentials of the MFCs with various cathodes have little differences, while the cathode potentials are greatly different. The electrochemical reaction rates could be evaluated by the open circuit potential (OCP), as Logan et al. [26] indicated, a higher OCP value is related to a higher reaction rate. In agreement with the result of OCV, the OCP of the MnO_2/GNS cathode at a loading of 5.0 mg cm^{-2} (0.303 V) is much higher than those of MnO_2 (0.118 V) and non-catalyst (0.09 V) cathodes, and also higher than that of Pt/C cathode at a loading of 0.5 mg cm^{-2} (0.261 V), evidently indicating that the performance of MnO_2/GNS cathode is enhanced due to the use of MnO_2/GNS nanocomposite as catalyst for ORR.

MnO_2 has previously been used as a cost-effective electrocatalyst for ORR in MFCs [10,14,16,27]. However, the performance of MFC with MnO_2 as cathode catalyst for ORR was slightly lower than that of the MFC with Pt/C as cathode catalyst under the same condition. In contrast to the prior work, the maximum power density of the MFC with MnO_2/GNS cathode at a loading of 5.0 mg cm^{-2} is 21.53% higher than that of Pt/C cathode at a loading of 0.5 mg cm^{-2}. The excellent performance of the MFC with MnO_2/GNS cathode is attributed to the improvement of the catalytic activity of MnO_2/GNS composite catalyst for ORR.

In contrast to conventional carbon supported electrocatalyst, the higher catalytic activity of the MnO_2/GNS results from good electrical properties of the GNS and the unique structure of MnO_2/GNS composite. The special two-dimensional structure of GNS, with its high surface area and conductivity, has been demonstrated to be advantageous as catalyst support material for the electrocatalyst. More importantly, the outstanding structure of MnO_2/GNS composite prepared by the method in our study plays an important role in the improvement of the catalytic activity. Due to the reaction between GNS and MnO_4^-, the decreased particle size and the improved dispersion of MnO_2 over the surfaces of the GNS provide a much larger catalyst surface area available for ORR and improve the utilization of MnO_2. Furthermore, the strong interaction and the increased contact area between MnO_2 and GNS greatly promote the catalyst stability and the electrical conductivity, thus facilitating electron transfer and improving the cathode performance. In addition, oxygen may reach the surface of the MnO_2/GNS composite catalyst easily, resulting in the decrease of diffusion resistance, probably due to two-dimensional structure of GNS and nanoscale MnO_2 particles. Therefore, the mechanism of MnO_2/GNS for ORR is more complicated, further studies should be needed to understand its mechanism in order to optimize the performance of the system.

4. Conclusions

The nanostructured δ-MnO_2/GNS composite was prepared through a direct redox reaction between graphene and potassium permanganate under microwave irradiation. The electrode modified by MnO_2/GNS composite exhibited high catalytic activity for ORR due to excellent electrical properties of the GNS and the unique structure of MnO_2/GNS composite. Furthermore, the maximum power density of 2083 mW m^{-2} obtained with MnO_2/GNS catalyst was 1.42 and 1.22 fold higher than those of pure MnO_2 and Pt/C, respectively. The results demonstrate that MnO_2/GNS composite is a good alternative cathode catalyst to Pt in practical MFC applications.

Acknowledgments

The authors gratefully acknowledge the financial support provided by China Postdoctoral Science Foundation (20100480975 and special support), Fundamental Research funds for the Central Universities, and Heilongjiang Postdoctoral Science Foundation.

References

[1] B.E. Logan, Nat. Rev. Microb. 7 (2009) 375–381.
[2] S. Cheng, H. Liu, B.E. Logan, Electrochem. Commun. 8 (2006) 489–494.
[3] Y. Qiao, S. Bao, C. Li, Energy 3 (2010) 544–553.
[4] H. Wang, Z. Wu, A. Plaseied, P. Jenkins, L. Simpson, C. Engtrakul, Z. Ren, J. Power Sources 196 (2011) 7465–7469.
[5] H.R. Yazdi, S.M. Carver, A.D. Christy, O.H. Tuovinen, J. Power Sources 180 (2008) 683–694.
[6] F. Harnisch, S. Wirth, U. Schröder, Electrochem, Commun. 11 (2009) 2253–2256.
[7] Y. Yuan, B. Zhao, Y. Jeon, S. Zhong, S. Zhou, S. Kim, Bioresour. Technol. 102 (2011) 5849–5854.
[8] J.R. Kim, J.Y. Kim, S.B. Han, K.W. Park, G.D. Saratale, S.E. Oh, Bioresour. Technol. 102 (2011) 342–347.
[9] L. Deng, M. Zhou, C. Liu, L. Liu, C. Liu, S. Dong, Talanta 81 (2010) 444–448.
[10] X. Li, B. Hu, S. Suib, Y. Lei, B. Li, J. Power Sources 195 (2010) 2586–2591.
[11] I. Roche, K. Scott, Appl. Electrochem 39 (2009) 197–204.
[12] K. Gong, P. Yu, L. Su, S. Xiong, L. Mao, J. Phys. Chem. C 111 (2007) 1882–1887.
[13] F. Cheng, J. Shen, W. Ji, Z. Tao, J. Chen, ACS Appl. Mater. Interfaces 1 (2009) 460–466.
[14] L. Zhang, C. Liu, L. Zhuang, W. Li, S. Zhou, J. Zhang, Biosens. Bioelectron. 24 (2009) 2825–2829.
[15] X.W. Liu, X.F. Sun, Y.X. Huang, G.P. Sheng, K. Zhou, R.J. Zeng, F. Dong, S.G. Wang, A.W. Xu, Z.H. Tong, H.Q. Yu, Water Res. 44 (2010) 5298–5305.
[16] Y. Zhang, Y. Hua, S. Li, J. Sun, B. Hou, J. Power Sources 196 (2011) 9284–9289.
[17] A.E. Fischer, K.A. Pettigrew, D.R. Rolison, R.M. Stroud, J.W. Long, Nano Lett. 7 (2007) 281–286.
[18] N. Jovi, D. Dudi, A. Montone, M.A. Vittori, M. Mitri, V. Djokovi, Ultramicroscopy 108 (2008) 885–892.
[19] L. Xiao, J. Damien, J. Luo, H.D. Jang, J. Huang, Z. He, J. Power Sources 208 (2012) 187–192.
[20] W.S. Hummers, R.E. Offeman, Chem. Soc. 80 (1958) 1339–1341.
[21] J. Yan, T. Wei, B. Shao, Z.J. Fan, W.Z. Qian, M.L. Zhang, F. Wei, Carbon 48 (2010) 3825–3833.
[22] H. Liu, B.E. Logan, Environ. Sci. Technol. 38 (2004) 4040–4046.
[23] Q. Wen, Y. Wu, D.X. Cao, L.X. Zhao, Q. Sun, Bioresour. Technol. 100 (2009) 4171–4175.
[24] S.B. Ma, K.Y. Ahn, E.S. Lee, K.H. Oh, K.B. Kim, Carbon 45 (2007) 375–382.
[25] A.J. Bard, L.R. Faulkner, Electrochemical Methods: Fundamentals and Applications, second ed., John Wiley & Sons, New York, 2001.
[26] B.E. Logan, C. Shaoan, L. Hong, Electrochem. Commun. 8 (2006) 489–494.
[27] M. Lu, S. Kharkwal, H.Y. Ng, S.F. Yau Li, Biosens. Bioelectron. 26 (2011) 4728–4732.